Regular Article

Aerial firefighting system for suppression of incipient cladding fires

Mohamad S. Chehadeh[1,2] ⓘ, **Mohammad Wahbah**[1,2] ⓘ, **Mohammad I. Awad**[1,3] ⓘ,
Oussama AbdulHay[1] ⓘ, **Khalil Al Handawi**[4] ⓘ, **Lakmal Seneviratne**[1] ⓘ, **Ian Greatbatch**[5] ⓘ
and Yahya Zweiri[1,2] ⓘ

[1]Center for Autonomous Robotic Systems, Khalifa University, Abu Dhabi, UAE
[2]Department of Aerospace Engineering, Khalifa University, Abu Dhabi, UAE
[3]Healthcare Engineering Innovation Center, Department of Biomedical Engineering, Khalifa University, Abu Dhabi, UAE
[4]Department of Mechanical Engineering, McGill University, Montréal, Canada
[5]School of the Environment, Geography and Geosciences, University of Portsmouth, Portsmouth, UK

Abstract: Fires occurring at the exterior of high-rise buildings can be hard to tackle using current firefighting technology and tactics. Accessing fires at high floors is difficult, and can often result in delays in fire suppression, which in turn may lead to an uncontrollable fire. This paper proposes a semiautomated system of multiple, aerial robots that can suppress incipient cladding fires in high-rise buildings. Each developed UAV has six litres of pressurised aqueous film-forming foam (AFFF) solution, a two degrees of freedom nozzle, a thermal imaging camera (TIC), and an automated algorithm that can efficiently spread the extinguishing material. To maximize payload delivery and minimize response time, we also developed a semi-autonomous firefighting system (SAFS) that compensates for platform movements, wind, and pressure drop in the fire extinguisher. Experimental results support the effectiveness and the applicability of the proposed solution. Dual UAVs cooperate to suppress Class A wood crib fires of size 10A (est. 825 kW) and frontal area of more than one square metre imitating an exterior cladding fire in its incipient stage. In addition, the developed firefighting UAV was used in Challenge 3 of the Mohammad Bin Zayed International Robotics Competition (MBZIRC) 2020, where it delivered the highest amount of extinguishant to façade fires of any participating team.

Keywords: robotic fire suppression, firefighting visual servoing, robotic fire detection, thermal seeking nozzle, firefighting unmanned aerial vehicle, firefighting swarm

1. Introduction

Exterior cladding fires are a relatively recent phenomenon and have provided a severe challenge to existing firefighting strategies and systems. Fire safety systems have been used for decades to

suppress and even combat interior fires in high-rise buildings. However, gaining access to exterior fires at higher floors is limited by the reach of existing ladders, or requires a team to attack the fire from inside the building. Cladding fire incidents have been reported in UAE, UK, China and others (Badam, 2012; Bannister, 2015; Barakat, 2016; Flumenbaum, 2009; Pasha-Robinson, 2018; Stanton, 2015) with the Grenfell Tower incident being notably severe, with a death toll of 72 people (Lane, 2018). For these reasons, there is some interest in exterior cladding fires, especially concerning the fire dynamics and propagation behaviours of these fires (Blake et al., 2018; Chen et al., 2019; Livkiss, 2020; McLaggan et al., 2020). In general, exterior wall assemblies consist of some common components. These are the insulation layer fixed to the building's exterior wall (made from plastics like polystyrene (EPS), polyisocyanurate (PIR) or polyurethane (PU), or made of less combustible materials such as rock wool, glass wool, etc.), followed by an air gap, and lastly by metal composite material (MCM) panels. The MCM panels consists of an insulator, usually polyethylene, sandwiched between two thin metal sheets. Figure 1 shows an exploded view of a typical exterior wall assembly used in high-rise buildings.

A common metal used in MCM panel construction is aluminium, and as such they are often referred to as "aluminium composite panels" (ACP). ACPs are blamed for the fast spread of Tecom Building Fire (van Leijen, 2013), Lacrosse Building Fire (Hanmer, 2019), and The Address Fire (Chen et al., 2019). The flammability of ACPs depends on the combination of panel core used, air gap, and insulator (Livkiss, 2020; Matthew & Guillermo, 2018). The flammability trends of ACPs were analysed in details by numerous researchers (Blake et al., 2018; Chen et al., 2019; Matthew & Guillermo, 2018; McLaggan et al., 2020) who all observed accelerated propagation of a cladding fire once fully developed. In Chen et al. (2019), the accelerated propagation was attributed to rapid surface propagation, gaps between MCM and insulator, and fire re-entry through windows and other openings.

Combustible Components

Exterior wall assemblies exist in a range of configurations, but many include the same elements found on London's Grenfell Tower

AIR GAP
In many assemblies using insulation board and MCM panels, an air gap exists between the two components, which in a fire can aid in funneling flames up the sides of a building.

METAL COMPOSITE MATERIAL (MCM) PANELS
Aluminum is a common metal used for MCM panels, which are often referred to as "cladding." In combustible exterior wall assemblies, a plastic like polyethylene is sandwiched between two thin metal sheets to create the MCM panels.

FOAM INSULATION BOARD
An insulation layer is applied directly to the building's exterior wall. Commonly used plastics like polyisocyanurate, believed to have been used on Grenfell Tower, are cheaper than insulating materials such as rock wool or glass wool but are combustible.
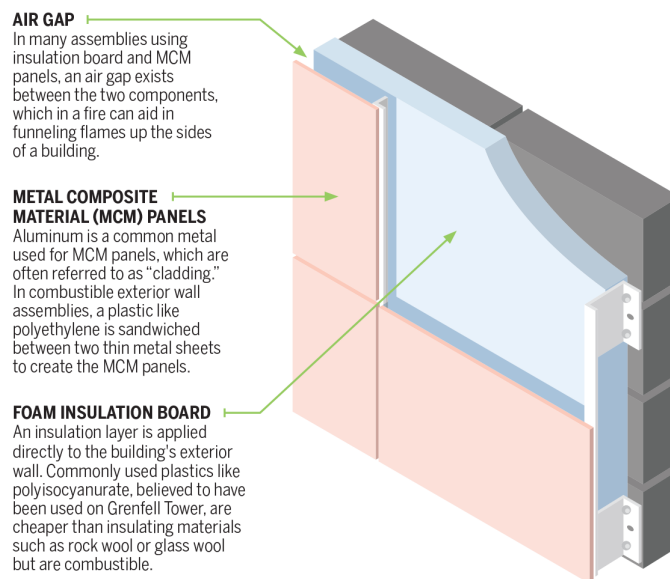
Figure 1. Exploded view of a typical cladding setup used for high-rise buildings. Address Downtown, Dubai, used ACP cladding with polyethylene core. *Source*: Reuters

Figure 2. A picture showing fire of the Address Downtown, Dubai, which happened during the celebrations of 2017 new year's eve. Source: In-Dubai

Interestingly, a cladding fire takes around 10 to 15 minutes from the moment of ignition to reach the rapid propagation phase (Chen et al., 2019). Blake et al. (2018) validated Fire Dynamics Simulator (FDS) software experimentally and found that a cladding fire, simulating the Grenfell Tower conditions, took around 450 s (7.5 minutes) to reach level two starting from level one of a two-story building. A more controlled experiment using a microscale combustion calorimetry (MCC) to analyse thermal decomposition of cladding material was conducted by McKenna et al. (2019) where the rapid increase of heat release rate (HRR) started after 450 s of ignition for multiple composite materials. Similar delayed rapid growth of HRR behaviour was reported by other research groups (Guillaume et al., 2018; McLaggan et al., 2020). The Address Downtown fire displayed similar propagation delay of fire, where a smoking LED mounted for New Year's Eve celebrations was blamed for the start of the fire (A picture of the fire is shown in Figure 2). The electrically sparked incipient fire was visible through CCTV cameras for about 15 minutes (Barakat, 2016). Unfortunately, the incipient fire location was out of reach. A small fire extinguisher could have contained or completely extinguished the fire during that incipient stage.

To address these challenges, we have developed a robotic firefighting system of multiple UAVs. Each is fitted with a modified standard AFFF extinguishers shown in Figure 4, and can quickly reach incipient fires at otherwise unreachable heights. In ideal conditions, these UAVs can reach a fire location at 1000 m altitude in around four minutes.

1.1. Existing firefighting robots

To date, few UAVs or robots have been developed for firefighting tasks, and even fewer efforts focus on speed and accuracy as required for incipient cladding fires. Based on our review, none of the currently documented systems provide autonomous, real time ability to combat large, incipient, cladding fires with multiple UAVs. For example, ZHUN, a firefighting UAV developed by Walkera Technology (Walkera Technology, 2020) carries a three kilogram firefighting powder payload with the design goal of reaching indoor fires at high altitudes through windows or similar openings. Because ZHUN was designed for confined space fires, targeting the fire base with accuracy is not a necessity. A tethered UAV from Aerones employs a manually controlled pan-tilt nozzle for firefighting aiming (Ibekwe,

2018). A downside of the Aerones UAV is that it puts a practical limit on the maximal achievable altitude due to its tether weight. The tether also introduces other movement constraints and hazards especially when operating in urban canyons or in the situation where a fire is located on the opposite side of a building. The Aerones manually controlled pan-tilt nozzle used to guide the extinguisher comes at the cost of placing additional requirements on the pilot. In McNeil and Lattimer (2017), a handheld robotic firefighting system was developed where a stereo thermal vision was used to localise spray trajectory and correct for errors, in real time. The operation of this handheld robot was limited to fires smaller than extinguishant spread (i.e. pinpoint fires). Ground robots, handheld robots, and other types of robots were also used to combat different fire scenarios (Amano et al., 2001; McNeil & Lattimer, 2017; Qin et al., 2016; Yuan et al., 2015).

1.2. Contribution

The firefighting UAV system presented in this paper uses a single thermal imaging camera (TIC) to locate the base of the fire, a frequency-modulated continuous-wave radar sensor to measure the nozzle distance to the cladding, and a novel algorithm to guide a two degrees of freedom (2DOF) nozzle. These components together form the Semi-Autonomous Firefighting System (SAFS). The contributions in the developed firefighting UAV are multifold:

- A multi-UAV system is used to tackle larger incipient fires, minimising response time due to UAV agility and software that can autonomously navigate to fire location based on user inputs to a 3D building model.
- A novel pan-tilt nozzle controlled by SAFS is used to compensate for uncontrolled UAV movements. Our design is more complex than the handheld pan-tilt mechanism in McNeil and Lattimer (2017), due to the alignment of the TIC with the UAV body frame which configuration adds 9-DOF to the aiming problem. Coping with such complexity is required to achieve accurate aiming since the amount of extinguishant available on-board is limited.
- The ability of SAFS to handle larger fires while accounting for extinguishant trajectories and external wind. SAFS divides a large fire into smaller ones and fights them according to a strategy predefined by the pilot. Therefore, each firefighting UAV only requires a single pilot, due to the automation of the firefighting nozzle.

2. The design of the UAV for firefighting missions

In this section, we discuss the major design choices considered in developing the multi-UAV firefighting system. The design goals can be stated as follows:

- Reach the fire location as quickly as possible. In other words, minimise the time between receiving firefighting request to the start of firefighting.
- Deliver payload to the fire as accurately as possible, mimicking behaviour of a human firefighter.

These design goals are in line with the nature of incipient cladding fires, where the fire development to uncontrollable blaze can be avoided within 15 minutes of fire start. The design requirements are hence defined as:

- Minimum reachable altitude (relative to takeoff) of 828 m (the height of Burj Khalifa, Dubai).
- Ability to extinguish at least a Class A fire with size 5A (NSAI, 2007) representing incipient cladding fire.

We start by defining some specific firefighting performance terminology. The time to take-off T_t is the time from fire detection and reporting to UAV takeoff, including, if applicable, time to replace an exhausted extinguisher. The time to reach T_r is the time from UAV take-off to reaching fire

site. We also define time to engage T_e to be the time from reaching fire site to the beginning of extinguishant ejection. These three time intervals, when summed up, give the total response time T_{res}. The total response time T_{res} is of particular interest to firefighting professionals. Other performance measures include the time to completely deplete the extinguisher T_d, and the time to extinguish the fire T_f, which starts once the first UAV engages in firefighting and ends when the fire is completely extinguished. Lastly, we define the total mission time from the moment of fire reporting till the complete extinguishing of the fire to be $T_{tot} = T_{res} + T_f$. These firefighting performance parameters are illustrated in the flowchart presented in Figure 6.

2.1. Tethered vs. non-tethered UAVs

The purpose of the tether system is to provide the firefighting UAV system with constant supply of power and extinguishant. Based on the utilisation of a tether system, firefighting UAV Systems can be categorised into tethered and non-tethered systems. Tethered UAV design has been extensively addressed in literature for a variety of applications (Kiribayashi et al., 2018; Tognon & Franchi, 2017; Yibo et al., 2013). The proposed system falls under the non-tethered category. We believe that a non-tethered system is more suitable to combat fires for high-rise buildings, as it allows more agility, and larger flight envelope. Despite the fact that a tether system would virtually enable infinite operation, it would limit the UAV's flight envelope, disabling it from reaching higher altitudes. Moreover, for high-rise buildings application, a tethered UAV severely impacts time to reach, T_r, and puts practical limitations on the reach and stability of the UAV, hence jeopardising the reliability of the firefighting solution. An overall comparison between tethered and non-tethered UAV designs for firefighting is shown in Table 1.

Furthermore, to illustrate the in-feasibility of applying tethered solution for high-rise building firefighting applications, we consider a best-case tethered UAV design with a hose connection of $1 \, cm^2$ cross section, having an extinguishant with specific gravity of one, hose weight of $100 \, g/m$, and power tether weight of $10 \, g/m$. Considering the highest required altitude of $828 \, m$ the tether weight would be $173.88 \, kg$ thus requiring a massive UAV to complete the operation.

## 2.2. A single large UAV versus multiple smaller UAVs

Theoretically, any given extinguishant payload could be fitted onto either a single large UAV or alternatively be divided across multiple smaller UAVs. In our proposed system, we chose multiple UAVs over a single large UAV. Additionally, we have developed and demonstrated the use of multiple UAVs concept using two UAVs. Our selection is based on the advantages of using multiple UAVs which are shown in Table 2. Furthermore, by reducing T_t, T_r, and T_e for each UAV in the fleet of UAVs and by having sufficient number of UAVs, the use of multiple UAVs can provide almost continuous

Table 1. Comparing tethered versus non-tethered UAVs for firefighting missions.

Criteria	Tethered UAV (full extension condition)	Non-tethered UAV
Flight time	Virtually infinite	Limited
Extinguishant supply	Virtually infinite	Limited
Flight envelope	Limited by the tether. It cannot reach all building surfaces	Exceeds most required scenarios
Withstanding wind	Dangerous because of tether swing	Can withstand high speeds of wind
Manoeuvrable	Low because of the large inertia	More agility enabling quicker operation
Redundancy	Complex and unsafe to use multiple UAVs resulting in no redundancy	Can be made redundant by using multiple UAVs
Regulatory approval	Hard due to the large size and weight	Easier

Table 2. Comparing a single large UAV versus multiple smaller UAVs for firefighting missions.

Criteria	A single large UAV	Multi-UAVs
Regulatory approval	Harder	Easier
Redundancy	Impractical	Redundant by design
Crash severity	High	Low
Agility	Less agile	High
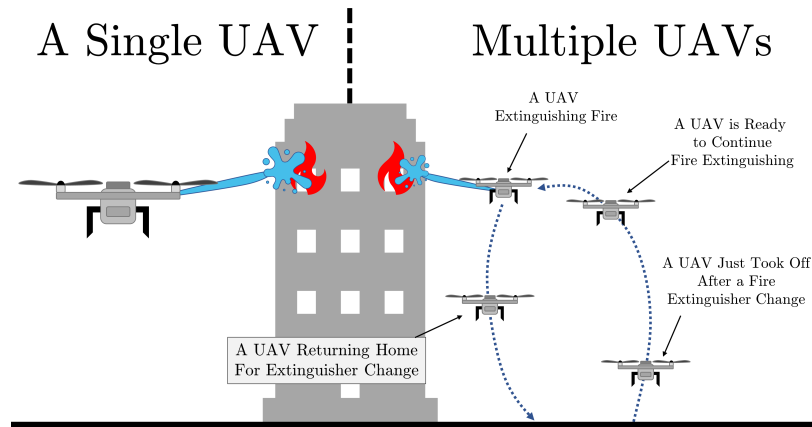
Figure 3. Illustration of the concept of using multiple UAVs compared to using a single larger UAV.

delivery of extinguishant to the fire target as compared to a single large UAV with matching payload capability (Figure 3).

2.3. Design choices for firefighting

To narrow selection criteria of UAVs, we have considered a number of limitations, such as firefighting components. AFFF Foam was chosen as extinguishant medium based on its performance specifically with incipient cladding fires. Common options for foam propulsion include pre-pressurised containers or pumping using an electric pump. Pumping has two advantages over pre-pressurised containers. Firstly, with pumping, extinguishant can be refilled easily by the operator allowing for quicker preparation of the firefighting UAV. Secondly, pumped extinguishant has an almost constant stream trajectory, and so hitting the target would be easier and more precise. However, our experiments revealed that pre-pressurised containers are more weight efficient for on-board foam quantity of less than 10 L and that SAFS can compensate for the pressure drop in pre-pressurised containers. Therefore, pre-pressurised containers were chosen. P50F Composite fire extinguishers, produced by Britannia Fire Ltd. have the highest extinguishant to extinguisher weight ratio on the market and are available in 2 L, 6 L, and 9 L sizes, weighing 2.8 kg, 8.5 kg and 11.7 kg respectively.

We have also developed a method for quickly replacing depleted extinguishers. It is also worth noting that the selected fire extinguisher was designed for vertical operation, whereas it needs to be operated horizontally when carried by the UAV as shown in Figure 4. Thus we have changed the fire extinguisher internal suction nozzle as illustrated in Figure 5. The modification had no effect on the discharge characteristics of the extinguisher (discharge time, extinguishant residuals in the extinguisher, etc.), when comparing vertical and horizontal operation.

The nozzle was given 2DOF to adjust both pitch and yaw to compensate for uncontrolled UAV movements resulting from external wind, and sensors noise. Furthermore, the angle of the nozzle aiming point can be adjusted according to pressure drops in the extinguisher, external wind conditions,
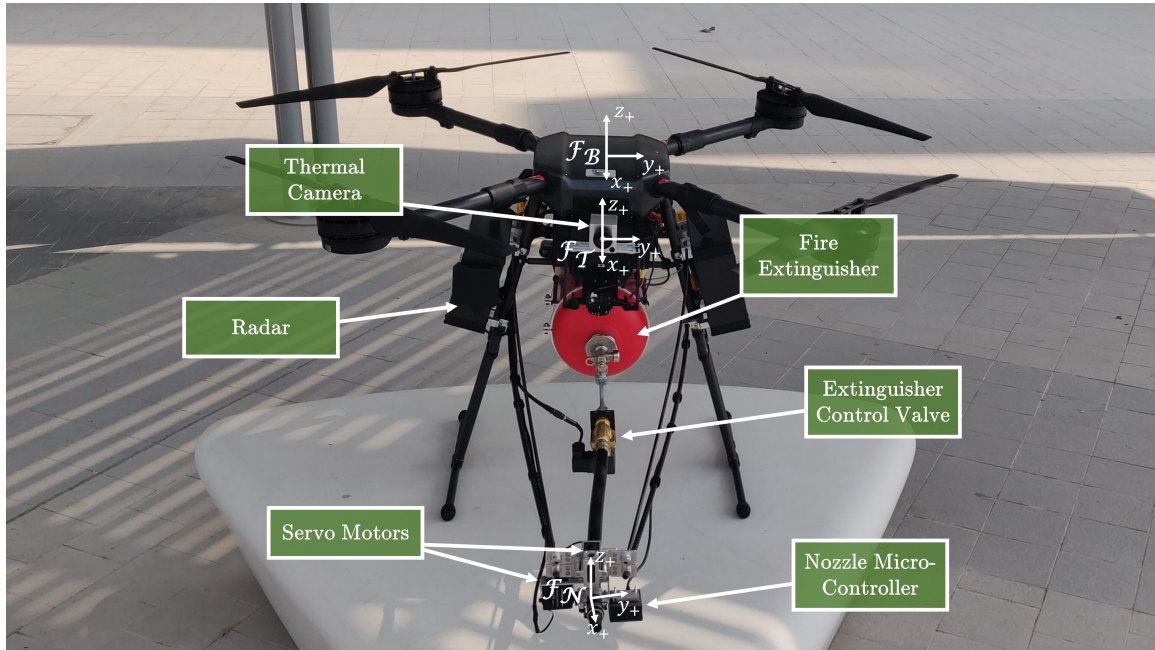
Figure 4. A front-view picture of the firefighting UAV developed at Khalifa University highlighting key firefighting components and showing reference frames attached to the UAV body, to the TIC, and to the nozzle.
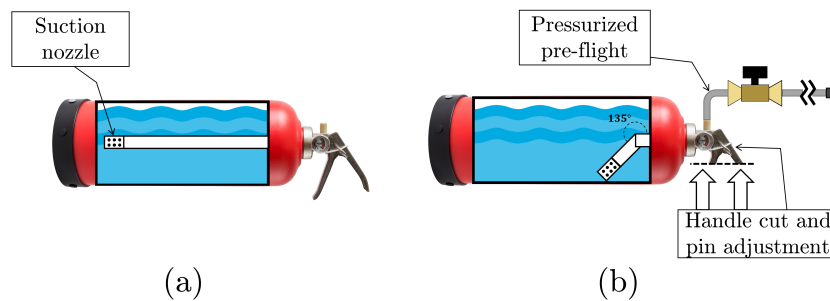

Figure 5. An illustration showing the modification applied to the extinguisher internal suction nozzle. (a) An off the shelf Britannia P50F 6 L foam fire extinguisher. (b) The extinguisher is modified for maximum efficiency during horizontal operation. The handle was cut for space constraints and additional hole was drilled in the handle to hold it in the pressed position.

and distance to fire, which increases operator aiming accuracy. This is achieved via SAFS, discussed in the following section. The extinguisher nozzle needs to be placed away from the rotors' disk in order that air flow from the rotors does not disturb the extinguishant stream. Because multirotor UAVs are symmetric, it was important to keep the centre of mass (CoM) at the geometric centre of the UAV to utilise full capacity of the motors. However, the extinguisher nozzle needs to be placed away from the UAV body and as close to the fire base as possible. Our solution was to offset the fire extinguisher placement in the direction opposite to the nozzle to compensate the CoM offset. By placing the nozzle further away from the UAV body, the nozzle gets closer to the fire base without endangering the UAV.

Table 3. Some mechanical specifications of the developed firefighting UAV based on DJI Wind4 platform. Field tests where done near to sea levels.

Specification	Value	Notes
Extinguishant payload	6 litres	After modification total take-off weight of 27 kg
Flight time	18 minutes	Hovering with full payload
Wind resistance	12 m/s	Field tested for up to 8 m/s
Climbing speed	5 m/s	Field tested up to 60 m. Reaches 828 m in 165 s or 2.75 min (calculations)
Descending speed	3 m/s	Field tested from 60 m to ground level

2.4. Selection of the UAV platform and overall system design

The market of UAVs with takeoff weights of less than 50 kg is relatively mature and provides several options for custom and ready-to-fly UAVs. To simplify regulatory approvals required, developmental efforts of the UAV, and the burden of testing a custom developed UAV, a ready-to-fly UAV was chosen for this project. Based on our weight calculations, we found that the DJI Wind4 UAV platform would be capable of lifting the 6 L P50F extinguisher as well as all other required avionics and sub-systems presented in this paper (DJI, 2018). This choice met the minimum design requirements while maximising design aims. The DJI Wind4 platform is capable of interfacing with custom developed software thus allowing for customised firefighting features. The DJI Wind4 platform was modified to have two batteries which increases flight time, allowing multiple sequential operations by changing the fire extinguisher and a relaunch without requiring a system restart. One of the developed firefighting UAVs is shown in Figure 4. Specifications for the developed Firefighting UAV are shown in Table 3.

2.5. Autonomous navigation to fire location

To minimise reaction time to fire calls, we have designed a user interface with a 3D model of the guarded tower(s) that responds to user touch inputs to generate trajectory points for autonomous takeoff and navigation to the fire site. This 3D model is part of the ground control station (GCS) which provides the ground operator with full control over the operation, and displays information key to the success of the firefighting mission. In an extended scenario, multiple UAVs can be placed near to high-rise buildings where they can autonomously respond to fire alarms initiated by human operators. The automation of GPS navigation from take-off to reaching the fire site yields lower T_t and T_r performance parameters compared to manual flight, keeps the user focused on firefighting aspects, and minimises the number of pilots needed to operate multiple UAVs. Safety during navigation is maintained using radar distance measurements for obstacle avoidance and by allowing the user to manually override operation at any instant. To achieve autonomous navigation relative to a fixed structure, we define two reference frames $\mathcal{F}_\mathcal{G}$ and $\mathcal{F}_\mathcal{I}$ to be the global, and the inertial reference frames respectively. $\mathcal{F}_\mathcal{G}$ is a GPS frame (WGS 84 is used) with heading referenced to the magnetic north. The inertial frame is in SI units and is calibrated and defined on site. The calibration aligns two acquired GPS locations with two calibrated points away from the tower base. We have tested this experimentally based on Emirate Civil Defence Academy (ECDA) training tower where we have developed a model for the building and have done the calibration on site. It is important to take GPS error margins specific to the deployment location into account. GCS software allows the user to check generated waypoints and calibration on a world map. Waypoints generation workflow through GCS and $\mathcal{F}_\mathcal{G}$ to $\mathcal{F}_\mathcal{I}$ calibration are explained in the Appendix. Additionally, the video in Chehadeh et al. (2019a) shows a demonstration of the mission planning capability of the GCS applied to the firefighting training tower in the ECDA training facility, UAE.

It is important to emphasise that the calibration step need be performed only once, at system installation. For subsequent uses, the firefighting UAV can take off immediately after the fire location on the building façade is selected. We found this feature to significantly reduce T_r especially in cases where the firefighting UAV is beyond the operator line-of-sight (LOS). Once the firefighting UAV
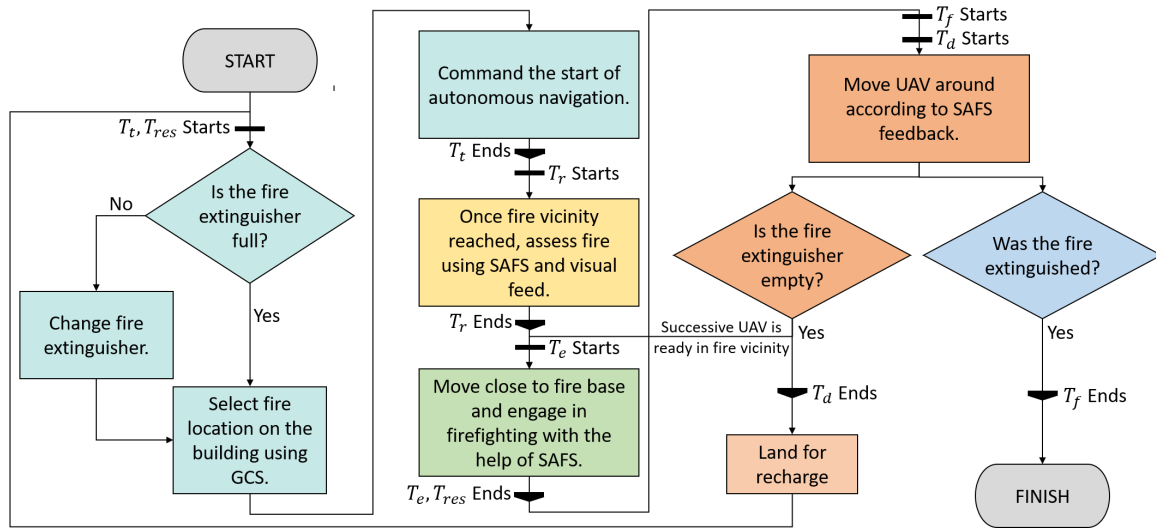
Figure 6. A diagram showing typical mission flow. Key time performance metrics are related to the mission stages. Quick fire extinguisher changing mechanism, and intuitive UI design shortens T_t. GPS based navigation reduces T_r especially in out of line-of-sight cases. SAFS contributes to the reduction of T_e and T_d, and the increase of firefighting efficiency.

reaches the vicinity of fire by GPS autonomous navigation, the flight mode changes to manual control and SAFS is activated for the firefighting operation.

Another benefit of navigation automation through GPS is that it reduces the number of operators needed for multiple UAVs. The human operator is only required to perform firefighting operations, and when a fire extinguisher is depleted, another UAV will be at the fire site ready for the firefighting pilot to take over. Figure 6 presents a modal firefighting operational scenario, where the relation between GPS Navigation, SAFS operation, and timed performance parameters is shown.

3. The Semi-Autonomous Firefighting System

Our team conducted a few early stage experiments in ECDA training facility on a multistory building that has multiple openings. In one of these experiments a standard wood crib fire target was set on a window opening at ten meters height. The expert pilot could not extinguish the fire as most of the extinguishant missed the fire target. The results of this experience has set the motivation for the development of the Semi-Autonomous Firefighting System (SAFS). We believe that the main strength of the proposed design over other possible solutions found in literature is the inclusion of SAFS. This system automates nozzle aiming at fire sources, thus eliminating the need for the operator to compensate for:

- UAV position drift due to sensors' noise and external wind.
- External wind and earth gravity affecting the extinguishant stream.
- Change of extinguishant trajectory profile due to pressure drop in the fire extinguisher.
- Human error in the alignment of the nozzle observed from visual feedback.

SAFS encompasses various sub-systems and components, as can be seen in Figure 7. The On-Board Computer (OBC) carries the main logic behind the SAFS algorithms and acts as a communication hub, connecting all sub-components. The OBC hardware is an Intel NUC NUC7I7DNBE and runs Linux Ubuntu 16.04 with Robot Operating System (ROS) and DJI On-board Software Development
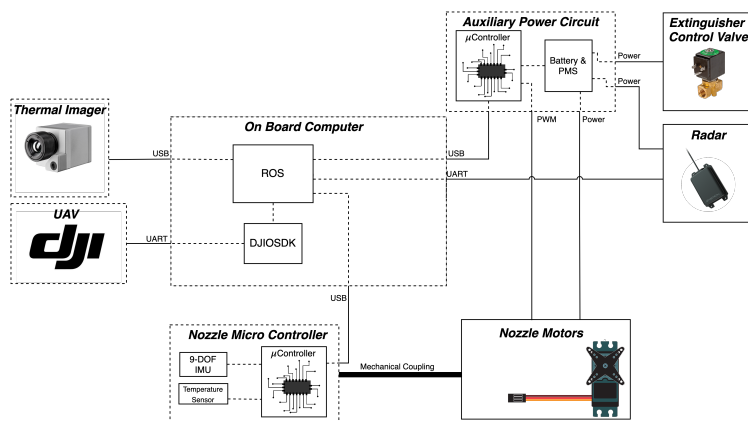
Figure 7. SAFS system level diagram showing power and signal interconnections.

Kit (OSDK). The Auxiliary Power Circuit (APC) sub-system, which contains a micro-controller (SAMD21), a Li-Po battery, and a Power Management System (PMS), is responsible for actuating the servo motors (ProTower MG995) and the valve, while also providing power to the radar. The Nozzle Micro-Controller (NMC) hosts an Inertial Measurement Unit (IMU) with 9 Degrees of Freedom (MPU-9250) and provides real-time readings of the nozzle orientation. The TIC (Optris PI200), which has a 160×120 resolution and is equipped with a $41° \times 31°$ FOV lens, is also connected to the OBC, and it provides real-time thermal readings necessary to track the fire base. The last major component of the SAFS is the radar (Ainstein SRD-D1) which provides accurate distance to the obstacle facing the UAV which is assumed to be the fire.

The SAFS operation can be split into three successive stages:

- Fire Detection and Segmentation.
- Generating Nozzle Reference Angles.
- Nozzle Control and State Estimation.

Additionally, the SAFS constantly receives user commands and provides operational information to the Ground Control Station (GCS), making it an essential part of the SAFS operation.

3.1. Fire detection and segmentation

While in operation, the SAFS analyses images captured by the TIC of fire sources. A heat source is considered to be a fire if any temperature reading at any given pixel is above a certain temperature threshold σ_t, and for the wood fire selected for our experiments, we have found that $\sigma_t = 330\,°C$ masks out flames and only detects fire fuel (i.e. the wood). For optimum accuracy, this value can be adjusted depending on cladding type of the guarded building.

Once a fire is detected within the TIC field of view (FOV), the SAFS then assesses the fire size. The detection algorithm starts by applying σ_t threshold to all pixels in the view followed by the application of Canny edge detector to remove outliers based on area size. The total faced area of the fire A_{tot} and the perimeter are then calculated in pixel's units. Since the available data is that of a mono-TIC (i.e. they do not provide depth information), radar distance readings d_r are used to convert area in pixels into square metres. This is possible by taking the TIC FOV parameters into consideration while assuming the side projected distance between the UAV nozzle and the fire base constant across the whole TIC FOV. This assumption is reasonable for buildings with generally flat outer surfaces.

Knowing the total fire area allows the SAFS to split the fire into smaller areas that can be covered by the extinguishant spread. The segmentation is performed along the horizontal axis of the thermal image, with the assumption that the fire hasn't spread significantly, due to its incipient nature. The segmentation was chosen to be performed horizontally because of multiple observations, the first of which is that extinguishant cross sectional profile becomes elongated in the dimension perpendicular to the earth surface due to gravity, more evidently the larger distance it travels, thus providing good vertical coverage to tackle fires of the incipient nature. Gravity also causes the extinguishant foam to trickle down the building facade which also aids in covering bigger vertical area, and suppressing vertical spread. Additionally, controlling the UAV altitude is an easier task for the operator, compared to horizontal manoeuvres, which require rolling action in this case, thus the horizontal segmentation makes more sense. Finally, this approach mimics the technique used by human firefighters, which procedure consists of targeting the base of the fire, followed by horizontal sweep as the fire gets extinguished (also commonly known as pull, aim, squeeze, sweep technique). An approximate extinguishant area of effect (A_{eff}) was deduced experimentally from the spread of the extinguishant stream as a function of nozzle distance to fire, and fire extinguisher pressure as shown in Figure 9. The value of (A_{eff}) was used to calculate the number of segments $|S|$ the fire will be split into by using the following equation:

$$|S| = \begin{cases} \lceil \frac{A_{\text{tot}}}{A_{\text{eff}}} \rceil & A_{\text{tot}} > A_{\text{eff}} \\ 1 & A_{\text{eff}} \geq A_{\text{tot}} > A_{\text{min}} \\ 0 & A_{\text{min}} \geq A_{\text{tot}} \end{cases} \tag{1}$$

Each segment in the set $S = \{s_1, \ldots, s_{|S|}\}$ will then be tackled on its own. Once the fire is extinguished in that segment, the algorithm tackles the next adjacent segment. Segmentation can be challenging in some cases which must be handled carefully. For example, multiple disjoint fires can be present in the camera FOV. For that case SAFS handles fire disjoint and only considers segments corresponding to fire base. The SAFS will start targeting the leftmost segment (Left To Right (LTR) mode) or the rightmost segment (Right To Left (RTL) mode), depending on the wind direction set by the operator. For example, if the wind direction is from the left, relative to the nozzle, LTR operation mode will be selected by SAFS. The user has the option to override this setting (i.e. manual choice of LTR or RTL modes). The next step is to target the centre of the targeted segment, determined by a two dimensional pixel location. Let $f_{\text{WGC}} : S \to P$ where $f_{\text{WGC}}(S) = \{\vec{p_s} \mid s \in S\}$ be a function mapping that uses weighted geometric centre (WGC) to find the vector $\vec{p_s} \in P$ that defines a pixel coordinates corresponding to the target for each segment. WGC was preferred over geometric centre as it provides better extinguishing efficiency since it prioritises hotter areas of the fire. The WGC of each fire segment is computed using the following equation:

$$\vec{p_s} = \begin{bmatrix} p_x \\ p_y \end{bmatrix} = \frac{1}{C} \begin{bmatrix} \sum_{i=1}^{W} i \sum_{j=1}^{H} p_{ij} \\ \sum_{i=1}^{H} i \sum_{j=1}^{W} p_{ij} \end{bmatrix} - \begin{bmatrix} \frac{W}{2} \\ \frac{H}{2} \end{bmatrix}, \quad C = \sum_{i=1}^{W} \sum_{j=1}^{H} p_{ij} \tag{2}$$

where W is the width of the image in pixels, H is the height of the image in pixels, p_{ij} corresponds to the pixel intensity located at the ith column and the jth row of the image. Figure 8 provides an example of how SAFS processes raw TIC input.

3.2. Generating nozzle reference angles

It is necessary to translate the targeted pixel location p_s in the currently targeted fire segment to nozzle reference angles. This needs to be carefully done due to the existence of multiple reference frames and error sources. We define reference frames $\mathcal{F}_\mathcal{B}, \mathcal{F}_\mathcal{T}$, and $\mathcal{F}_\mathcal{N}$ corresponding to the body, TIC, and nozzle frames respectively. We use right handed coordinate system with $x(+)$ aligned with: the front of the UAV, view direction of the camera, and default calibrated nozzle position for every corresponding reference frame. These reference frames are shown in Figure 4. The calibration
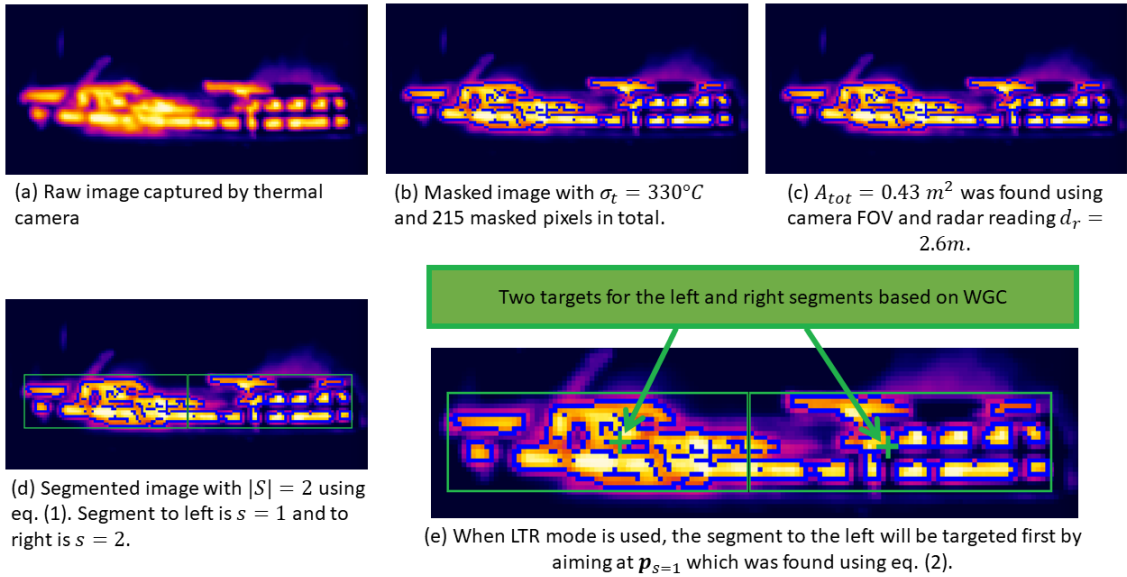
(a) Raw image captured by thermal camera

(b) Masked image with $\sigma_t = 330°C$ and 215 masked pixels in total.

(c) $A_{tot} = 0.43\ m^2$ was found using camera FOV and radar reading $d_r = 2.6m$.

(d) Segmented image with $|S| = 2$ using eq. (1). Segment to left is $s = 1$ and to right is $s = 2$.

Two targets for the left and right segments based on WGC

(e) When LTR mode is used, the segment to the left will be targeted first by aiming at $\boldsymbol{p}_{s=1}$ which was found using eq. (2).

Figure 8. A breakdown of the fire detection and segmentation stages. The shown example shows how an actual wood fire is perceived by the SAFS.

between the reference frames is essential for payload delivery accuracy. Calibration terms determine rotational and translational offsets between reference frames in the rest state. Therefore we define a pose transformation in the three dimensional space by:

$$T = \left(\begin{array}{c|c} \boldsymbol{R} & \boldsymbol{t} \\ \hline \boldsymbol{0} & 1 \end{array} \right) \tag{3}$$

where $\boldsymbol{T} \in \boldsymbol{SE}(3)$ is a 4×4 matrix in the special euclidean group, $\boldsymbol{R} \in \boldsymbol{SO}(3)$ is a 3×3 matrix in the special orthogonal group, and $t \in \mathbb{R}^3$ is a three dimensional position. An example transformation from reference frame $\mathcal{F}_\mathcal{B}$ to $\mathcal{F}_\mathcal{T}$ is represented by ${}^\mathcal{T}_\mathcal{B}\boldsymbol{T}$. The frames $\mathcal{F}_\mathcal{B}$ and $\mathcal{F}_\mathcal{T}$ are rigidly linked with known translational offset from the system's CAD model. $\mathcal{F}_\mathcal{N}$ is flexible with respect to other frames due to attachment compliance. Calibration term ${}^\mathcal{N}_\mathcal{T}\bar{\boldsymbol{T}}(t_0)$ is obtained by placing a laser pointer instead of the nozzle and aligning it with a projected parallel line corresponding to the centre pixels in the TIC. Since the aforementioned method provides $\mathcal{F}_\mathcal{N}$ to $\mathcal{F}_\mathcal{T}$ calibration along the yaw and pitch axes, the roll calibration was performed mechanically through the design of the holding mechanism, which consists of two pairs of carbon rods, with each pair equal in length and placed equidistantly to the drone body, thus providing tension on the nozzle assembly that eliminates rolling of $\mathcal{F}_\mathcal{N}$ w.r.t. $\mathcal{F}_\mathcal{T}$, as seen in Figure 4. The parameter t_0 represents the dependency of the calibration terms on the nozzle IMU temperature. A calibration lookup Table that contains the nozzle gyro and accelerometer bias dependencies on temperature is obtained and applied based on current IMU temperature measurements. Nozzle compass soft-iron and hard-iron calibration is done as described in Fang et al. (2011). As a result of these calibrations, full knowledge of ${}^\mathcal{N}_\mathcal{T}\bar{\boldsymbol{T}}(t_0)$ is obtained. This transformation is applied to raw measurements and when transforming quantities among reference frames.

Let us define generic Euler orientation state vector to be $\Theta = [\theta, \phi, \psi]^T$ where θ, ϕ and ψ being the pitch, roll and yaw angles respectively. TIC optical specifications can be linearized to approximately

map $\vec{p_s}$ to the corresponding nozzle reference angles Θ_r in the reference frame $\mathcal{F}_\mathcal{T}$:

$$\Theta_r = \begin{bmatrix} \tan^{-1}\left(\frac{d_r\tan(p_y V_F/H)-b_x}{d_r-b_y}\right) \\ 0 \\ \tan^{-1}\left(\frac{d_r\tan(p_x H_F/W)-b_z}{d_r-b_y}\right) \end{bmatrix} + \boldsymbol{E}(_\mathcal{T}^\mathcal{N}\bar{\boldsymbol{T}}(t_0)) + \Theta_c(\hat{p}(t),\vec{w},d_r) \tag{4}$$

where the H_F and V_F correspond to the horizontal and the vertical fields of view of the camera, in degrees, respectively, b_x, b_y and b_z are the geometric offsets between $\mathcal{F}_\mathcal{T}$ with respect to $\mathcal{F}_\mathcal{B}$ origin and is derived from CAD drawings, $\boldsymbol{E}(_\mathcal{T}^\mathcal{N}\bar{\boldsymbol{T}}(t_0))$ maps the rotation matrix in $_\mathcal{T}^\mathcal{N}\bar{\boldsymbol{T}}(t_0)$ to Euler angles, and Θ_c corresponds to the correction angles accounting for extinguishant trajectory dynamics. The nozzle correction angles Θ_c take into account estimated pressure level in the extinguisher $\hat{p}(t)$, external side wind vector $\vec{w}$, and distance to wall reported by radar d_r (d_r is equivalent to distance from nozzle).

The values of Θ_c were found through two experiments. In the first experiment, extinguishant projectile characteristics in no-wind conditions were measured. A few extinguishers were depleted in a setup imitating in-flight conditions and the nozzle placed parallel to the ground plane. Projectile behaviour of the extinguishant due to gravity was recorded as a function of the distance to nozzle and pressure drop in the extinguisher. Pressure drop was assumed to be a function of time since extinguishing started. Initial pressure conditions are assumed identical across different extinguisher containers. This experiment results in a lookup table that takes $\hat{p}(t)$ and d_r as input and outputs corresponding Θ_c. A photo taken during this experiment is shown in Figure 9. Measurements from five valid experiments were used in the results presented in Table 4.

The second experiment investigated the effect of a side wind source on the side deviations of the extinguishant trajectory. An anemometer was used to provide a set of calibrated wind speed measurements produced by an artificial wind source (outdoor industrial fans). The wind speed produced by the fans were adjusted by varying the fan rotational speed. A camera placed at a height provides top view of the extinguishant during the experiment. Using markers placed at ground, trajectory side deviations were recorded as a function of $\vec{w}$ and $\hat{p}(t)$. The lookup table for Θ_c is augmented with data from the side wind experiment and linear interpolation is used whenever applicable. As with the previous experiment, photometric measurements from a calibrated camera are used to estimate extinguishant trajectory behaviour, where the distance between the extinguishant trajectory and the background markers is assumed to be small. A photo taken during this experiment
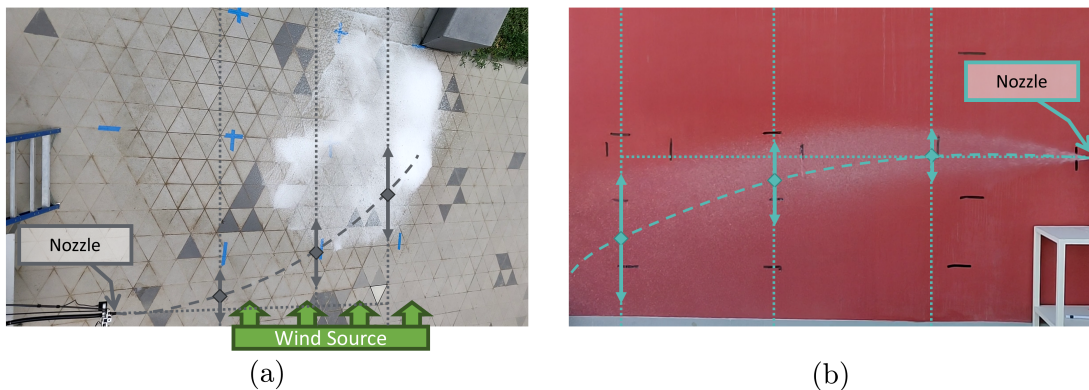

(a)   (b)

Figure 9. Experiments used to find extinguishant stream characteristics. In (a) side wind test is shown where green arrows indicate the direction of an induced wind stream with controlled varying speed up to 5 m/s. Extinguishant spread, and deviation angles are noted as a function of distance, time, and wind speed. In (b) the effects of gravity and extinguisher pressure drop on the stream trajectory are investigated. For this case extinguishant spread, and deviation angles are noted function of distance, and time.

Table 4. Experimental results showing the mean μ and the standard deviation σ for extinguishant trajectory subject to gravity and side wind as illustrated in Figure 9. Data are recorded at multiple values of time since trigger t_r and distance to nozzle d_r. Data are also recorded for $t_r = 5\,\text{s}$, $30\,\text{s}$ and $40\,\text{s}$. Full trajectory characterisation is obtained by linear interpolation and extrapolation.

Parameter	t_r (s)	0			10			20		
	d_r (m)	1	2	3	1	2	3	1	2	3
A_{eff} (m^2)	μ	0.049	0.066	0.102	0.067	0.203	0.322	0.073	0.231	0.470
	σ	0.015	0.018	0.021	0.019	0.032	0.040	0.016	0.046	0.049
Altitude drop due to	μ	0.03	0.02	0.09	0.11	0.15	0.22	0.14	0.18	0.41
gravity (m)	σ	0.001	0.001	0.001	0.001	0.008	0.011	0.009	0.014	0.026
Side deviation due to 3.5 m/s	μ	0.03	0.33	0.51	0.09	0.39	0.67	0.12	0.37	0.82
wind (m)	σ	0.001	0.006	0.011	0.002	0.009	0.019	0.005	0.012	0.026
Side deviation due to 5 m/s	μ	0.11	0.54	0.82	0.29	0.61	1.12	0.31	0.77	1.21
wind (m)	σ	0.002	0.009	0.018	0.005	0.011	0.025	0.004	0.015	0.032

is shown in Figure 9. Measurements from three valid experiments for each side wind speed were used in the results presented in Table 4.

3.3. Nozzle control and state estimation

Two servo motors were employed to actuate the nozzle (model used is LewanSoul LDX-218) which were internally controlled with a proportional controller. However, steady-state errors were observed in the alignment to nozzle reference angles Θ_r. This can be referred to the inner-servo dead-band and the undetermined tension of the fire hose. To compensate for this situation, an integral (I) controller was added to control the 2DOF nozzle servo motors. The I controller was tuned experimentally to provide quickest over-damped response of the system. An Anti-windup algorithm was used with the integrator term to mitigate windup and to keep the servo motors in acceptable operational limits (Astrom & Rundqwist, 1989).

The estimation of the nozzle angles $\hat{\Theta}_n$ used complementary filtering technique (Mahony et al., 2005). The complementary filter was used to fuse estimated angles from the accelerometer and the compass with the gyroscope readings (Mahony et al., 2005). An adjustment was performed on the yaw error $\bar{\psi}_{\text{err}}$ to ensure that the actuator always prefers the shortest path to the reference angle. This adjustment is given by the equation:

$$f_w(x) = \begin{cases} x + 2\pi & x < \pi \\ x - 2\pi & x > \pi \\ x & else \end{cases} \tag{5}$$

where the result is fed to the yaw integrating controller.

3.4. Ground Control Station feedback and UI

The user can adjust SAFS parameters and monitor system operation via the GCS. The GCS was designed to provide the ground operator with full control over the operation and displays information key to the success of the firefighting mission. SAFS operation begins once the UAV reaches the vicinity of the fire through autonomous GPS navigation. Using a visual camera stream and radar measurements that triggers a beeping audio feedback with variable frequency, the operator can safely navigate close to the fire. The SAFS detects the fire when it is within a specified distance from the UAV and the beeping alarm frequency will report adequate distance to fire (0.9 Hz to 1.5 Hz beeping frequency is used for adequate distance to fire). The operator has the choice to use SAFS or to

extinguish the fire manually (i.e. keep the nozzle at rest). The SAFS constantly displays the detected fire size in dm^2, the maximum detected fire temperature, the current number of fire segments $|S|$, the current radar reading d_r in centimetres, and the reading of a temperature sensor mounted at the nozzle, i.e. the closest point to the fire. These readings offer various benefits to the operator. For example, the change in fire size along with the number of fire segments can indicate to the operator whether the fire is being contained or if it is spreading. Another example is the reading of the temperature sensor mounted at the nozzle as it can warn the operator in case of flying dangerously close to the fire.

There are a plenty of other utility features that the GCS offers. The GCS is equipped with nozzle calibration settings, allowing the operator to calibrate the nozzle accelerometer, gyroscope, and magnetometer, as well as various SAFS settings, such as the wind speed, wind direction (at deployment stage, wind data will be retrieved in real-time through anemometers network already installed across Burj Khalifa), and firefighting approach direction (i.e. RTL or LTR). A detailed explanation of the SAFS settings window on the GCS is provided in the Appendix.

4. Experimental tests and results

The experimental tests aim to validate quantitatively and qualitatively the performance of the firefighting UAV with SAFS. First, a static test (i.e. without UAV flight) of the SAFS tracking feature was conducted in a controlled lab environment (discussed in subsection 4.1), followed by testing on an extinguishing accuracy apparatus showcasing the improvement of using the UAV with SAFS over using it without SAFS (discussed in subsection 4.2). Then field tests for the validation of the tracking accuracy without flight and with real fire were conducted (discussed in subsection 4.3). Finally, the UAV with SAFS was tested on an actual fire replicating the intended fire scenario as much as possible (discussed in subsection 4.4).

4.1. Static lab test

In this test, the Firefighting UAV was placed on a rigid base with the SAFS system mounted on it. In front of the UAV, a heated-steel plate was placed on a fixed distance within the FOV of the TIC. The plate was heated until it reached a temperature distinguishable by the TIC. The extinguisher hose was replaced by a laser pointer to better monitor the performance of the heat source tracking. Consequently, the extinguishant trajectory dynamic compensation term Θ_c was ignored in this test, since the aim was to assess the mechanism accuracy, isolated from external disturbances. The TIC detected the heated plate as a fire, and adjusted the number of segments to target, based on the distance and the mocked extinguisher state. The operator then activated the auto-targeting functionality, and the laser point location was compared to the actual set point as seen on the thermal image (refer to Figure 10 for illustration). To further test the system, an infrared blocking plastic sheet was inserted in front of the heated steel plate to simulate a fire being extinguished, and the performance of the SAFS fire segmentation feature as well as the nozzle tracking system response were observed. Figure 12 shows the tracking performance of the laser pointer to the desired reference generated by SAFS. In the considered scenario, the heated steel plate was exposed as a result of the infrared blocking plastic sheet being removed. Root-mean-square error (RMSE) for tracking was found to be 0.026 m, or 0.59°. A video capture of this test can be seen in Chehadeh et al. (2019c). A final test on the same setup was conducted, in which the UAV was tilted around its pitch axis, as well as a rotation around its yaw axis. In both cases, the tracking system performance was measured and was found to be satisfactory with measured RMSE of 0.091 m, or 2.05°. To benchmark these results, the minimum possible theoretical RMSE was calculated. By taking the motor Pulse Width Modulation (PWM), and the camera resolutions into consideration, the theoretical minimum was found to be 0.49°, which is close to the 0.59° in the first test.
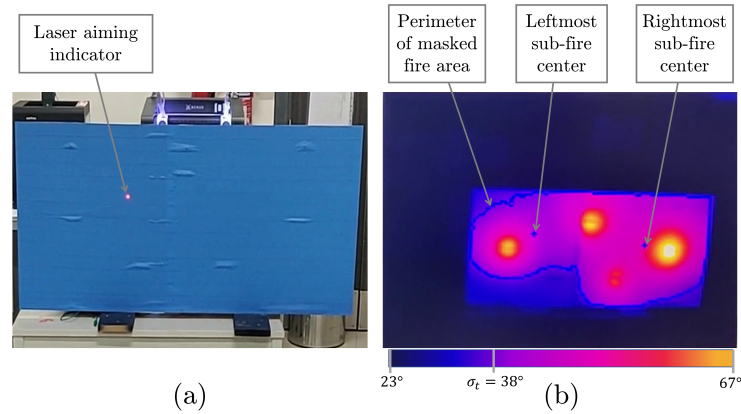
Figure 10. Test stand used for SAFS validation in lab environment. To the left is the heated steel plate with visible laser pointer indicating where SAFS is aiming. To the right is a screen showing the output of the SAFS fire detection algorithm where the whole heated plated is divided into two sub-fires, $|S| = 2$. Note the laser pointer is aiming to the centre of the left sub-fire, as SAFS is in LTR mode.
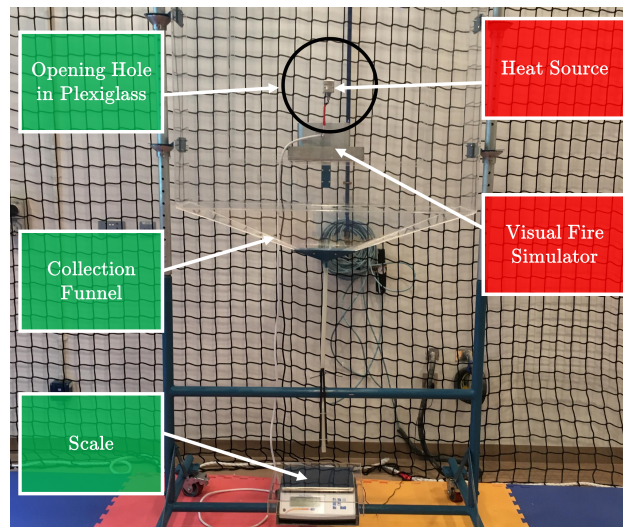

Figure 11. Test stand used to quantify accuracy of payload delivery to target. The test stand provides a target that is similar to façade fire targets used in MBZIRC2020.

4.2. Accuracy test for payload delivery

In this test, an apparatus consisting of a plexiglass box with an adjustable window size and height is used to collect the extinguishant from the UAV during a mock operation. The setup utilised a heating element placed in the centre of window to simulate a fire, and a funnel that collects the ejected extinguishant to a weighing scale placed on the bottom of the setup. The setup is shown in Figure 11. Two tests were carried out, the first with a pilot flying the UAV and manually trying to eject as much extinguishant as possible through the window without the use of the SAFS, while the other system relied on the SAFS to deliver as much of the payload as possible, while the pilot merely maintained the target within the FOV of the TIC. Extinguishers with similar capacities were used in both tests, with testing conditions of $v_{\text{wind}} = 0\,\text{m/s}$.
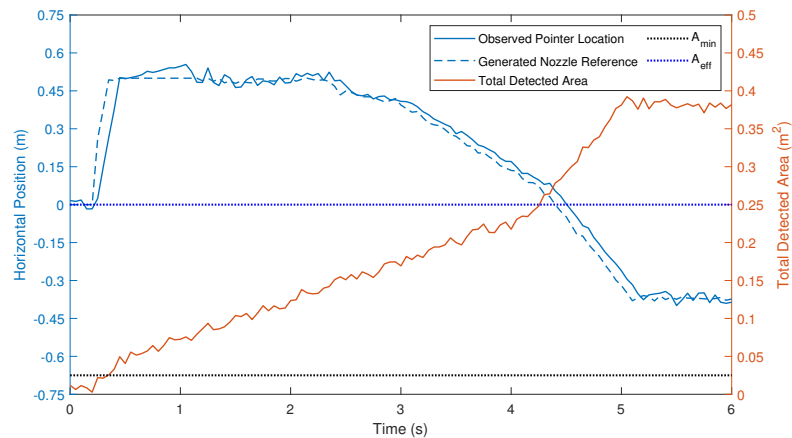
Figure 12. Reference following performance of SAFS on a growing simulated fire. No reference was generated by SAFS when $A_{\text{tot}} < A_{\text{min}}$. Total number of segments was $|S| = 1$ for the case when $A_{\text{tot}} > A_{\text{min}}$ and $|S| = 2$ for the case when $2A_{\text{eff}} > A_{\text{tot}} > A_{\text{eff}}$. Reported radar distance was $d_r = 2\,\text{m}$.

In the manual test, the initial release of the extinguishant proved to be the most wasteful, since the flow rate is the highest in the beginning, and the pilot doesn't have a knowledge about the extinguishant trajectory. Once the pilot adjusts the UAV position to successfully deliver the payload, the task of maintaining the position, as well as provide adjustments for gravity drop, and possibly wind effect remains. Since the pilot is only relying on the first person view (FPV) camera, these tasks proved to be challenging, since the extinguishant spread is big enough to partially cover the camera view and moving the UAV platform around is slow. The main advantage was in lowering the time its required to engage in firefighting.

When SAFS was used, we measured $T_e = 4.8\,\text{s}$ (averaged from three tests for all cases) while for manual operation we found $T_e = 11.7\,\text{s}$. The quantity delivered to target in the first three seconds (the heat source cools down and become undetectable due to extinguishant) of trigger using SAFS was $384\,\text{mL}$ with range of $88\,\text{mL}$ (three tests were conducted for each case). The quantity delivered to target in the first three seconds of trigger without SAFS was $263\,\text{mL}$ with range of $206\,\text{mL}$. In addition to accuracy of payload delivery and consistency in performance, the usage of SAFS was helpful from operational point of view as it provided an automated way of aiming at target thus allowing the pilot to better focus on more important aspects of the flight like planning and safety considerations.

4.3. Static fire test

This test comprised of placing the UAV approximately $0.75\,\text{m}$ above the ground, facing a fire that is placed $2\,\text{m}$ away from the nozzle on the same height. The fire width was approximately $1\,\text{m}$ and with a σ_t of $330\,^{\circ}\text{C}$. The SAFS system was set to automatic mode on the LTR setting. The ambient side wind speed was recorded for each test. Many experiments have been conducted to fine tune SAFS parameters. A video of an experiment with the tuned SAFS parameters can be found in Chehadeh et al. (2019b). The experiment shown in the video was a challenging one because of the high ambient wind speed $v_{\text{wind}} = 7\,\text{m/s}$. In this particular test, SAFS was in LTR mode, as the side wind direction was from the left, and it divided the fire into three segments. The accuracy shown in the video was not possible without the adjustments made by SAFS to compensate for wind speed and gravity drop effects. This experiment was repeated a few times with similar fire size where the fire was completely extinguished every time.

One important observation from this test was that sometimes there remained small spots of fire which are not extinguished. These small detectable fires can distract the SAFS and reduce firefighting efficiency, and hence we modified SAFS to exclude small isolated fire areas from SAFS operation (a small fire has a detected area less than $A_{\min}$). Those fire residuals can be targeted in manual mode towards the end of the firefighting operation as the UAV can then safely approach the fire.

4.4. Fire extinguishing scenario

This is the final test where wood is set on fire imitating a real fire scenario. We followed the fire and testing specifications stated in DIN EN3-7 standard (NSAI, 2007) as much as practically viable. We have followed this standard because we assume that class A fire will best represent outer cladding fires. Because of the physical limitation of the UAV firefighting scenario where fire can only be approached from one side, as opposed to the DIN EN3-7 standard where the fire base can be extinguished from any direction, we have reduced the depth of the reference wood crib. The physical difference between the wood crib referenced in the DIN EN3-7 standard and the one we used is shown in Figure 13. We denote the modified standard size with an asterisk as in 5A* for 5A equivalent fire. It is worth noting that the modified wood crib mass is 82% of that for the reference standard due to mechanical stability limits. We have used Pinus Silvestris wood sticks containing 10% to 15% of moisture by mass with wood stick density of $0.40\,\mathrm{kg\,dm^{-3}}$ to $0.65\,\mathrm{kg\,dm^{-3}}$ as specified in NSAI (2007). The relation between width parameters C_{w0} and C_{wi} is fixed as $C_{w0} = C_{wi} + 60\,\mathrm{mm}$ and the value of C_{wi} changes with the fire size by the relation $C_{wi} = 200x$ where x is the modified fire size xA* (e.g. for 5A* $C_{wi} = 200 \times 5 = 1000\,\mathrm{mm}$). The wood crib was mounted on a fire-resistant scaffolding at a height of 3 m. Once ignited, the fire in the wood crib is permitted to burn for eight minutes so that the fire is fully developed before extinguishing process starts. The pilot was restricted to use video feed for firefighting so that all obtained test results are valid for out of LOS fires. Figure 14 shows the setup used in this experiment.

We have done six tests (all without SAFS) with fire sizes 5A* and 10A* (three tests for each size), estimated to have peak HRR of around 413 kW and 825 kW respectively (Noaki et al., 2018). We have found that a single UAV is capable of suppressing at least 5A* fire. In some tests a single UAV
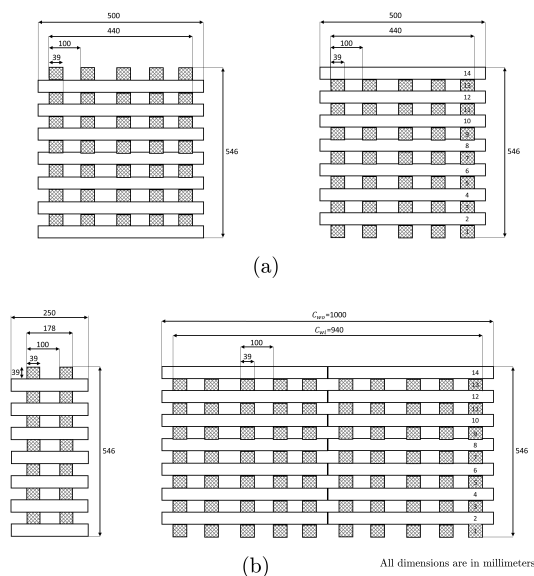

(a)

(b)

All dimensions are in millimeters

Figure 13. Reference drawing for standard and modified wood cribs of size (a) 5A and (b) 5A*.

Figure 14. Firefighting testing facility with a wood crib of size 10A* raised at three metres. A metallic back-plate is used to improve mechanical stability, and improve radar readings stability.

Table 5. Averaged results obtained using a single UAV to fight a 5A* fire and two UAVs to fight a 10A* fire. The test was repeated three times for each configuration. Typical firefighting scenario defined in Figure 6 was used for the calculation of firefighting performance metrics for each configuration.

Averaged Performance Measure	Single UAV tackling 5A* fire	Two UAVs tackling 10A* fire
Time to take-off T_t	40 s	40 s (First UAV)
Time to reach T_r	10 s	5 s (First UAV)
Time to engage T_e	9 s	12 s (averaged for the two UAVs)
Time to deplete T_d	60 s	50 s (averaged for the two UAVs)
Time to suppress fire T_f	60 s ($= T_d$)	112 s ($= 2T_d + T_e$)
Total mission time T_{tot}	119 s ($= T_f + T_e + T_r + T_t$)	169 s ($= T_f + T_e + T_r + T_t$)

was able to extinguish a 10A* fire on its own. On average, a single UAV is able suppress around 80% of a 10A* fire. A few tests were made with two UAVs trying to suppress a 10A* fire in successive manner showing the effectiveness of the multi-UAV approach in extinguishing fires. For these tests, the take-off position of the UAVs was ten metres away from the fire base. A video showing a single UAV suppressing a 5A* fire can be seen in Chehadeh et al. (2019d). Videos taken from different cameras for two of the multi-UAV firefighting tests can be found in Chehadeh et al. (2019e, 2019f).

An average of the firefighting performance for the conducted tests is shown in Table 5. Note that the T_r is considerably lower for the case of multiple UAVs since the latter UAV has already reached fire site when the former UAV was still extinguishing the fire. We have found from these tests that the wind gusts induced by the fire heat are significant when the fire is fully developed. These gusts make it very difficult for the pilot to keep the UAV in hover which might explain the slightly higher T_e required when tackling the larger 10A* fire. In addition, a considerable amount of extinguishant droplets get raised by such heat gusts and they further interact with the UAV propellers showering the UAV with these droplets (these effects can be clearly seen by the side-view cameras in the tests videos and are shown in Figure 15). No problems were observed because of this showering as the UAVs used were water resistant and nonflammable materials were used in UAV components. The time to deplete T_d for the single UAV case was slightly higher due to the different firefighting strategy compared to the two UAVs case as the smaller 5A* fire requires fine placement of the firefighting UAV. In total, the advantage of using multiple UAVs is evident by having higher fire mass per T_{tot} (having two UAVs increased time efficiency by a factor of 1.41 compared to the single UAV case). Combining the time figures that we got from these experiments with T_r figures tested separately for
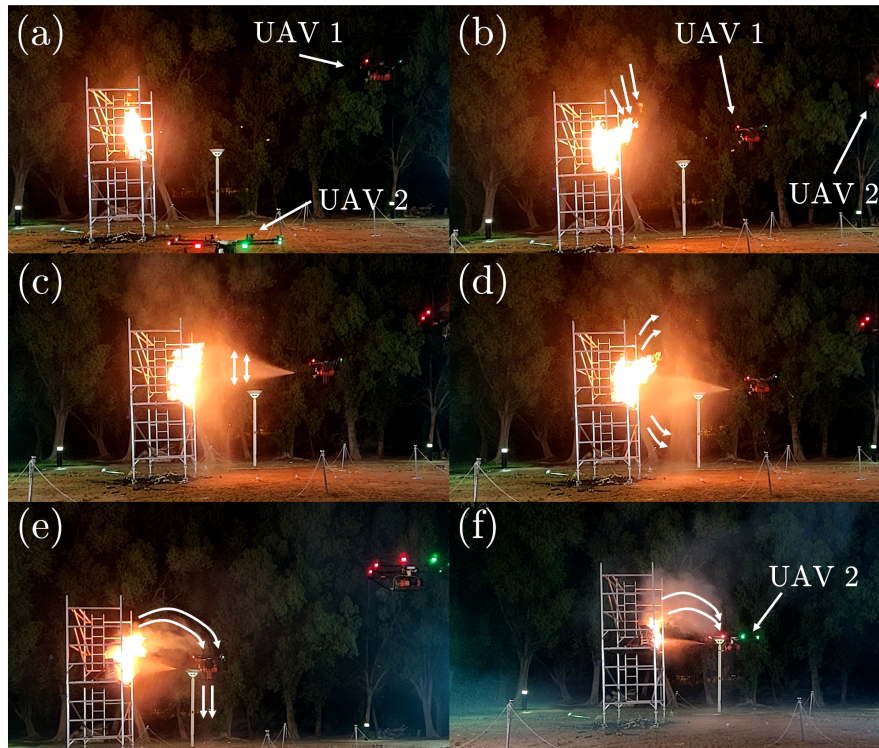
Figure 15. Side view captures from firefighting operation of 10A* fire. (a) The fire is fully developed and the flames are vertical as there is no wind. (b) Flames get sucked towards the UAV due to propulsion. (c) The extinguishant stream gets widened (compare with (d) and Figure 9 (b)) due to high pressure regions created by heat. The spread of the stream protects the UAV from fire heat and we found nozzle temperature to remain close to ambient temperature. (d) Shock waves are visible which are generated due to cooling effect created by extinguishant droplets. (e) Fire sparks, smoke, and extinguishant droplets are sucked by the UAV propellers showering the UAV body with fire sparks and water droplets. This emphasises the importance of using water and fire resistant materials in building the UAV. (f) The extinguishant stream is less spread as the fire is being contained.

high altitude incipient fires, we estimate total firefighting time for a 10A* fire requiring two UAVs at an altitude of 250 m to be $T_{tot} = 214\,s = 3.57\,min$. This is less than the time duration figures reported in literature for incipient cladding fire to become uncontrolled fire blaze (Blake et al., 2018; Chen et al., 2019; McKenna et al., 2019). Note that we have used the 250 m altitude figure as it was suggested by EMAAR that we can deploy the UAVs fleet at multiple locations in the middle of Burj Khalifa such that climbing the whole 828 m length of the Burj Khalifa is not necessary. If UAVs would be deployed solely at the ground level, total firefighting time would be $T_{tot} = 214\,s = 3.57\,min$.

A temperature sensor was placed at the nozzle tip to assure that the UAVs are not exposed to excessive heat during operation. We have found that no significant increase in observed temperature was observed even when the UAV was getting as close as 2.5 m to a fully developed 10A* fire. We concluded that the design requirements for heat-resistance materials can be relaxed for fire sizes similar to 10A*, while the focus shall be devoted to the design of a water-resistant UAV. Usage of flammable materials in the UAV body must be avoided due to fire sparks. Also, due to the fact that such fire sizes can be safely extinguished from distances at which the used fire extinguisher is effective, therefore a UAV design with longer nozzle hose is not required. Keeping the nozzle hose short increases weight efficiency, and maintains low vibration levels at the nozzle tip.

$$(a) \qquad\qquad (b)$$

Figure 16. Photos of the firefighting UAV targeting façade fires during MBZIRC2020. The fire in (a) is located at the second floor of the mock building used for Challenge 3. The fire in (b) is being targeted from a distance of about two meters.

Due to the ongoing COVID-19 circumstances, we were unable to conduct experimental firefighting tests with SAFS. Thus we are unable to provide comparative analysis of firefighting performance with and without the use of SAFS presented in the previous section.

4.5. Participation in Challenge 3 of MBZIRC2020

Al-Nokhba team, representing Khalifa University in MBZIRC2020, used the firefighting UAV presented in this paper to participate in Challenge 3 of MBZIRC2020. The team was led by the authors and consisted of Khalifa University researchers and local national service associates. Al-Nokhba team was placed fourth (tie) overall in the Grand Challenge and fourteenth overall in Challenge 3 (out of 20 teams). Challenge 3 involved the use of autonomous (or manual with penalty) ground and aerial vehicles in a firefighting scenario. In this challenge, Al-Nokhba team delivered the highest amount of extinguishant to the façade fire targets using UAVs with total delivered amount of 1000 mL (first floor target)+120 mL (second floor target)=1120 mL (first floor target received 1053 mL but the score cap per target is 1000 mL). The UAV was flown manually and SAFS was used to guide the nozzle to the fire centre. SAFS algorithm was re-purposed to cope with the nature of fire in the competition. SAFS was initially helpful in hitting the target accurately. However due to target cool down, the target became undetectable and SAFS switched to manual mode. Figure 16 shows a few photos of the developed firefighting UAV during MBZIRC2020.

4.6. Lessons learned

The design of firefighting UAVs can be quite challenging due to the variety of fire scenarios encountered in realistic conditions. Designing a firefighting UAV exclusively for targeting incipient stage cladding fires at high-rise buildings helped us focus our design goals and develop performance metrics that are appreciated by firefighting professionals. We have also received important feedback from our extensive testing, firefighting practitioners, and skilled UAV pilots, all of which helped us develop SAFS and get better idea about how to make this setup more practical. The main lessons learned can be summarised as follows:

1. Using an off-the-shelf UAV from DJI helped accelerate the development and have better focus on firefighting operational aspects. High level, complex navigation and planning algorithms can be added with ease to the platform through the DJI OSDK interface. Additionally, DJI mobile software development kit (MSDK) enabled networking across different platforms in the fleet.

We did encounter technical challenges, though, when we tried to rearrange the placement of components on the platform as the platform design blueprints are closed source (not available).

2. While it would be always beneficial to carry more payload by using larger UAVs, safety and regulatory constraints have to be taken into consideration. The swarming concept had effectively solved this issue. The swarm requires more efforts in software development aspects so that a single pilot can operate the whole fleet seamlessly.

3. Minimising the amount of wasted extinguishant is of utmost importance for firefighting efficiency, and hence SAFS was proposed. Side wind and gravity compensation proved especially useful for the initial hit of the fire source. This remains an open loop control structure and having a feedback through vision can be quite useful in consistently hitting fire target.

4. Some operational aspects related to firefighting shall get careful attention. For example we forget a few times to electrically connect the solenoid valve after replacing the fire extinguisher which caused firefighting mission to fail. We have avoided further occurrences of such situations by enforcing clear operational procedures with a pre-flight checklist. A better solution would be to install additional sensors which can confirm, through feedback signals, that all system components are connected prior to take-off.

5. Conclusion

This paper presented the detailed design, development, and testing of a UAV system for suppressing incipient exterior fires in high-rise buildings. Each UAV was equipped with an additional system called SAFS that makes the firefighting operation faster and more accurate. SAFS also makes the UAV easier to operate and offloads a lot of stress and effort from the ground operator. Experimental tests showed that multiple UAVs can be used to extinguish or contain larger incipient fires: The experiments showed that two UAVs can extinguish a fire of size 10A*. Most importantly, due to the quick response of the system, the proposed system contained the incipient cladding fires before they become uncontrollable.

By attacking and extinguishing fires in their incipient stages, our system offers the possibility of significantly reducing damage caused by exterior cladding fires. This capability have an obvious economic benefit, reducing the cost to residents, owners, insurance companies and ultimately regional economies, but also, and more importantly, reduce injury and death resulting from larger fires.

Future work will include making the firefighting operation using UAVs fully autonomous. This is important to make the swarming concept a reality. A few challenges need to be solved to achieve such capability, and here we list three major challenges:

- A 3D map of the fire scene that can be used to track fire propagation and provide accurate localization of UAVs through SLAM is needed. Such map can improve both safety and efficiency of firefighting.
- The second challenge that needs to be addressed is the closed-loop tracking of extinguishant trajectory using vision sensors. Guiding trajectory without feedback as discussed in this paper proved to be useful especially for the initial phase of extinguishant ejection, but its limitation in coping with uncertainty and varying environment conditions are obvious. The work of McNeil and Lattimer (2017) serves as a first step in this research direction.
- The last challenge is related to the software and hardware design aspects for a system that keeps the human operator fully aware of the firefighting mission. The ability to provide firefighting decisions in real time, both at high level and low level if needed, without disrupting the autonomous mission is of utmost importance for a life-saving firefighting scenario. Overall, once the operation is made fully autonomous, a firefighting UAV fleet can be deployed at a scale providing a practical solution for fighting fires at high rise buildings. These UAVs can be deployed in urban forests providing effective quick first response to cladding fires.

Acknowledgments

ORCID

Mohamad S. Chehadeh ⓘ https://orcid.org/0000-0002-9430-3349
Mohammad Wahbah ⓘ https://orcid.org/0000-0003-1647-8546
Mohammad I. Awad ⓘ https://orcid.org/0000-0003-1576-5359
Oussama AbdulHay ⓘ https://orcid.org/0000-0001-8299-6021
Khalil Al Handawi ⓘ https://orcid.org/0000-0002-1277-2396
Lakmal Seneviratne ⓘ https://orcid.org/0000-0001-6405-8402
Ian Greatbatch ⓘ https://orcid.org/0000-0002-9560-8291
Yahya Zweiri ⓘ https://orcid.org/0000-0003-4331-7254

References

Amano, H., Osuka, K., & Tarn, T.-J. (2001). Development of vertically moving robot with gripping handrails for fire fighting. *Proceedings 2001 IEEE/RSJ International Conference on Intelligent Robots and Systems. Expanding the Societal Role of Robotics in the the Next Millennium (Cat. No. 01CH37180)*, *2*, 661–667. https://doi.org/10.1109/IROS.2001.976245

Astrom, K. J., & Rundqwist, L. (1989). Integrator windup and how to avoid it. *1989 American Control Conference*, 1693–1698. https://doi.org/10.23919/acc.1989.4790464

Badam, R. T. (2012, October 17). Life-saving action by fire heroes as Dubai building engulfed by flames. *The National*. Retrieved August 26, 2020, from https://www.thenational.ae/uae/life-saving-action-by-fire-heroes-as-dubai-building-engulfed-by-flames-1.474316

Bannister, A. (2015, February 24). Dubai inferno: 5 of history's worst skyscraper fires. *IFSEC Global*. Retrieved August 26, 2020, from https://www.ifsecglobal.com/fire-news/dubai-inferno-5-historys-worst-skyscraper-fires/

Barakat, N. (2016, January 20). Fire at address hotel on New Year's Eve caused by electrical fault: Dubai Police. *Gulf News*. Retrieved August 26, 2020, from https://gulfnews.com/uae/fire-at-address-hotel-on-new-years-eve-caused-by-electrical-fault-dubai-police-1.1656786#

Blake, P., Phylaktou, H., & Andrews, G. (2018, October 1–3). *Validating FDS against a full-scale fire test* [Conference presentation]. 4th Fire and Evacuation Modeling Technical Conference, Gaithersburg, MD, United States.

Chehadeh, M., Wahbah, M., Awad, M., Oussama, A., Seneviratne, L., & Zweiri, Y. (2019a). *Mission planning using GCS* [Video]. YouTube. https://youtu.be/5kcR3j6R0ME

Chehadeh, M., Wahbah, M., Awad, M., Oussama, A., Seneviratne, L., & Zweiri, Y. (2019b). *SAFS static fire test* [Video]. YouTube. https://youtu.be/vauY8NYLy6I

Chehadeh, M., Wahbah, M., Awad, M., Oussama, A., Seneviratne, L., & Zweiri, Y. (2019c). *Simulating fire extinguishing in the lab with SAFS* [Video]. YouTube. https://youtu.be/jCDwIOflIhs

Chehadeh, M., Wahbah, M., Awad, M., Oussama, A., Seneviratne, L., & Zweiri, Y. (2019d). *A single UAV extinguishing a fire* [Video]. YouTube. https://youtu.be/SzF8ThWLZUI

Chehadeh, M., Wahbah, M., Awad, M., Oussama, A., Seneviratne, L., & Zweiri, Y. (2019e). *Two UAVs extinguishing a fire (A)* [Video]. YouTube. https://youtu.be/V01fmiLUbdY

Chehadeh, M., Wahbah, M., Awad, M., Oussama, A., Seneviratne, L., & Zweiri, Y. (2019f). *Two UAVs extinguishing a fire (B)* [Video]. YouTube. https://youtu.be/mGgJ4uM4w0g

Chen, T. B. Y., Yuen, A. C. Y., Yeoh, G. H., Yang, W., & Chan, Q. N. (2019). Fire risk assessment of combustible exterior cladding using a collective numerical database. *Fire*, *2*(1), 11. https://doi.org/10.3390/fire2010011

DJI. (2018). *DJI Wind 4 Quadcopter Specifications* [Apparatus]. The Quadrocopter Company. Retrieved August 26, 2020, from https://shop.quadrocopter.com/DJI-Wind-4-Quadcopter__p_1847.html

Fang, J., Sun, H., Cao, J., Zhang, X., & Tao, Y. (2011). A novel calibration method of magnetic compass based on ellipsoid fitting. *IEEE Transactions on Instrumentation and Measurement*, *60*(6), 2053–2061. https://doi.org/10.1109/tim.2011.2115330

Flumenbaum, D. (2009, March 12). CCTV headquarters fire: Rem Koolhaas Tower in Beijing survives blaze (updated). *The Huffington Post*. Retrieved August 26, 2020, from https://www.huffpost.com/entry/cctv-building-on-fire-ico_n_165186

Guillaume, E., Fateh, T., Schillinger, R., Chiva, R., & Ukleja, S. (2018). Study of fire behaviour of facade mock-ups equipped with aluminium composite material-based claddings, using intermediate-scale test method. *Fire and Materials*, *42*(5), 561–577. https://doi.org/10.1002/fam.2635

Hanmer, G. (2019, March 5). Lacrosse fire ruling sends shudders through building industry consultants and governments. *The Conversation*. Retrieved August 26, 2020, from https://theconversation.com/lacrosse-fire-ruling-sends-shudders-through-building-industry-consultants-and-governments-112777

Ibekwe, D. (2018, April 3). A Latvian company is developing drones that can put out fires. *Business Insider*. Retrieved August 26, 2020, from https://www.businessinsider.com/aerones-firefighting-drones-2018-4

Kiribayashi, S., Yakushigawa, K., & Nagatani, K. (2018). Design and development of tether-powered multi-rotor micro unmanned aerial vehicle system for remote-controlled construction machine. In M. Hutter & R. Siegwart (Eds.), *Springer Proceedings in Advanced Robotics: Vol. 5. Field and Service Robotics* (pp. 637–648). Springer. https://doi.org/10.1007/978-3-319-67361-5_41

Lane, B. (2018, June 4). Dr Barbara Lane's expert report. *Grenfell Tower Inquiry*. Retrieved August 26, 2020, from https://www.grenfelltowerinquiry.org.uk/evidence/dr-barbara-lanes-expert-report

van Leijen, M. (2013, March 6). A year later, reconstruction of gutted high-rises hanging fire. *Emirates 24/7*. Retrieved August 26, 2020, from https://www.emirates247.com/news/emirates/a-year-later-reconstruction-of-gutted-high-rises-hanging-fire-2013-03-06-1.497476

Livkiss, K. (2020, February). *Fires in narrow construction cavities: Fire dynamics and material fire performance* (Doctoral dissertation). Division of Fire Safety Engineering, Lund University. Lund, Sweden. https://lup.lub.lu.se/search/ws/files/75629766/Thesis_Karlis_Livkiss.pdf

Mahony, R., Hamel, T., & Pflimlin, J.-M. (2005). Complementary filter design on the special orthogonal group SO(3). *Proceedings of the 44th IEEE Conference on Decision and Control*, 1477–1484. https://doi.org/10.1109/CDC.2005.1582367

Matthew, B., & Guillermo, R. (2018). Flammability and multi-objective performance of building façades: Towards optimum design. *International Journal of High-Rise Buildings*, *7*(4), 363–374. https://doi.org/10.21022/IJHRB.2018.7.4.363

McKenna, S. T., Jones, N., Peck, G., Dickens, K., Pawelec, W., Oradei, S., Harris, S., Stec, A. A., & Hull, T. R. (2019). Fire behaviour of modern façade materials – understanding the Grenfell Tower fire. *Journal of Hazardous Materials*, *368*, 115–123. https://doi.org/10.1016/j.jhazmat.2018.12.077

McLaggan, M. S., Hidalgo, J. P., Carrascal, J., Heitzmann, M. T., Osorio, A. F., & Torero, J. L. (2020). Flammability trends for a comprehensive array of cladding materials. *Fire Safety Journal*, *120*, 103133. https://doi.org/10.1016/j.firesaf.2020.103133

McNeil, J. G., & Lattimer, B. Y. (2017). Robotic fire suppression through autonomous feedback control. *Fire technology*, *53*(3), 1171–1199. https://doi.org/10.1007/s10694-016-0623-1

Noaki, M., Delichatsios, M. A., Yamaguchi, J.-i., & Ohmiya, Y. (2018). Heat release rate of wooden cribs with water application for fire suppression. *Fire Safety Journal*, *95*, 170–179. https://doi.org/10.1016/j.firesaf.2017.10.002

NSAI. (2007). *Portable fire extinguishers - part 7: Characteristics, performance requirements and test methods*. Version EN 3-7:2004+A1:2007. National Standards Authority of Ireland.

Pasha-Robinson, L. (2018, February 8). Cladding fitted to Grenfell Tower was never fire safety tested. *Independent*. Retrieved August 26, 2020, from https://www.independent.co.uk/news/uk/home-news/grenfell-tower-cladding-fire-safety-checked-acm-cladding-aluminium-composite-material-reynobond-a8200801.html

Qin, H., Cui, J. Q., Li, J., Bi, Y., Lan, M., Shan, M., Liu, W., Wang, K., Lin, F., Zhang, Y. F., & Chen, B. M. (2016). Design and implementation of an unmanned aerial vehicle for autonomous fire-fighting missions. *2016 12th IEEE International Conference on Control and Automation (ICCA)*, 62–67. https://doi.org/10.1109/icca.2016.7505253

Stanton, J. (2015, March 4). British flight attendant questioned over Dubai blaze that ripped through 86-storey tower as police reveal fire started in his apartment. *Daily Mail*. Retrieved August 26, 2020, from https://www.dailymail.co.uk/news/article-2979720/British-flight-attendant-questioned-Dubai-blaze-ripped-86-storey-tower-police-reveal-fire-started-apartment.html

Tognon, M., & Franchi, A. (2017). Dynamics, control, and estimation for aerial robots tethered by cables or bars. *IEEE Transactions on Robotics*, *33*(4), 834–845. https://doi.org/10.1109/tro.2017.2677915

Walkera Technology. (2020). *ZHUN Firefighting UAV* [Apparatus]. Guangzhou Walkera Technology. Retrieved August 26, 2020, from https://www.walkera.com/index.php/Goods/info/id/71.html

Yibo, L., Qiling, X., & Jianda, H. (2013). Modeling and PID control of tethered unmanned quadrotor helicopter. *Proceedings 2013 International Conference on Mechatronic Sciences, Electric Engineering and Computer (MEC)*, 258–262. https://doi.org/10.1109/mec.2013.6885080

Yuan, C., Zhang, Y., & Liu, Z. (2015). A survey on technologies for automatic forest fire monitoring, detection, and fighting using unmanned aerial vehicles and remote sensing techniques. *Canadian Journal of Forest Research*, *45*(7), 783–792. https://doi.org/10.1139/cjfr-2014-0347

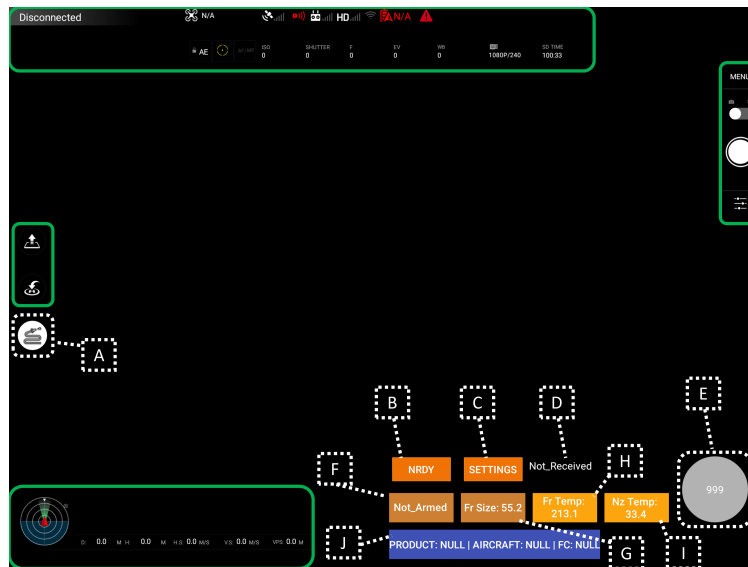## Appendix A. SAFS operation through GCS

Figure A1. The main screen used during firefighting operation where DJI UX elements are in green rectangles. Through (A) the user can navigate to nozzle settings screen. (B) shows the status of DJI OSDK mission, (C) navigates to mission settings screen shown in Figure B3, (D) shows the status of the mission sent from the 3D model, (E) displays the value of d_r in cm, (F) shows the status of the firefighting valve switch, (G) shows reported fire size in dm^2, (H) displays maximum reported fire temperature, (I) reports temperature reported at the nozzle, and (J) reports DJI OSDK and MSDK connection status.
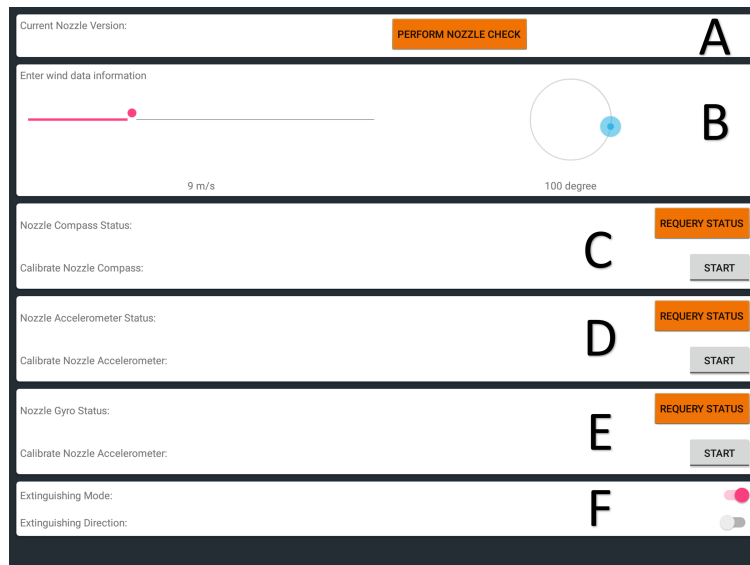
Figure A2. Nozzle settings UI screen where part (A) is used to perform nozzle system check, (B) is used to input ambient wind direction in $\mathcal{F}_\mathcal{N}$ frame, (C), (D) and (E) are used to perform nozzle sensors calibration, and (F) is used to enable/disable SAFS and to select either RTL or LTR firefighting modes.

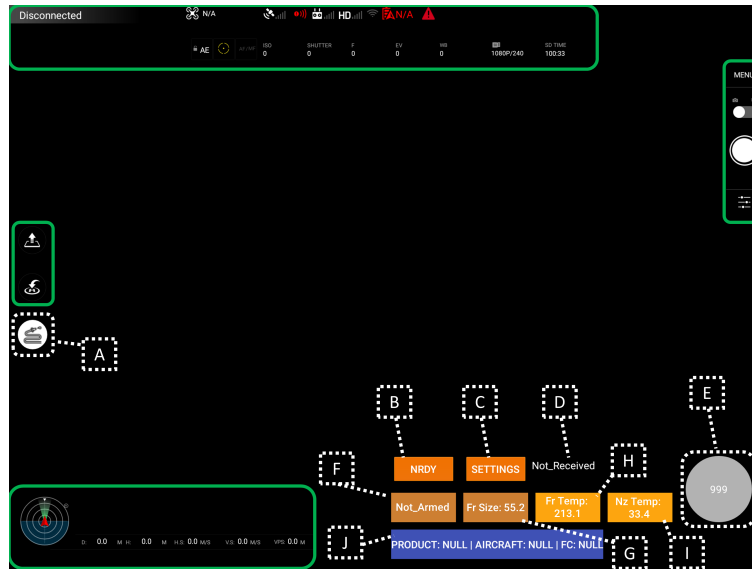## Appendix B. Autonomous GPS navigation through GCS

Figure B1. Illustration of the calibration points selection. The UAV is placed on each calibration point and GPS measurements are collected as shown in Figure B3.
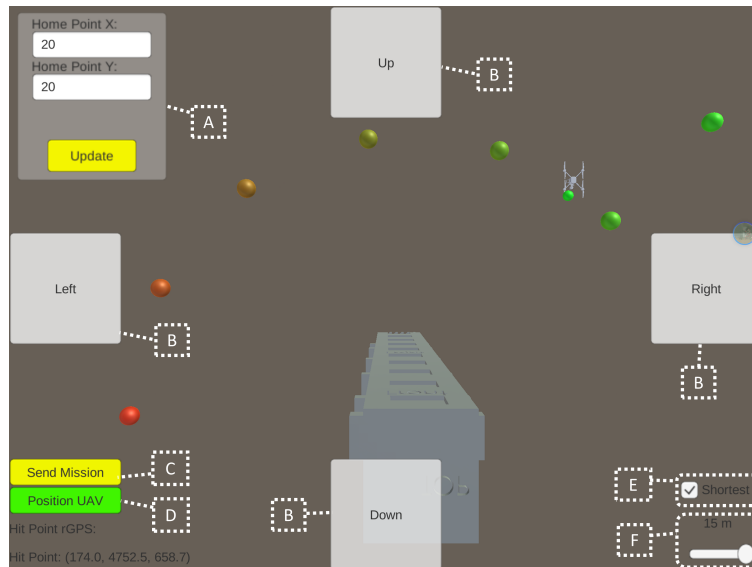

Figure B2. A 3D model of the ECDA training tower is used to generate UAV waypoints (shown as coloured spheres) based on user touches. In (A), UAV takeoff location can be assigned in the $\mathcal{F}_\mathcal{I}$ frame. In (B) user can navigate screen, and in (C) and (D) the user can send mission to UAV flight controller. In (E) and (F) rotation direction and radius around the building can be defined.
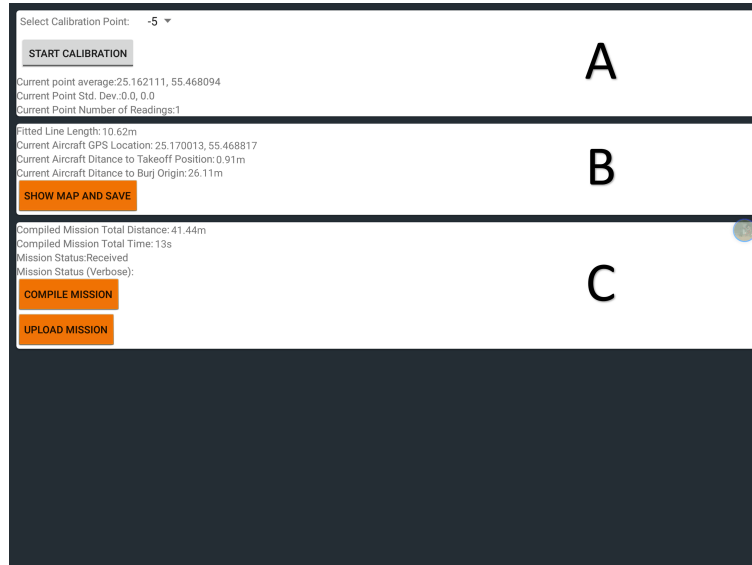
Figure B3. UI screen used for $\mathcal{F}_\mathcal{G}$ to $\mathcal{F}_\mathcal{I}$ calibration. (A) GPS measurements for two calibration points at a predefined measured distance are collected (as illustrated in Figure B1). (B) then validation measurements and validation through map can be done as shown in Figure B4. In (C) the mission can be uploaded to DJI Wind4 flight controller and total mission time and distance are displayed.
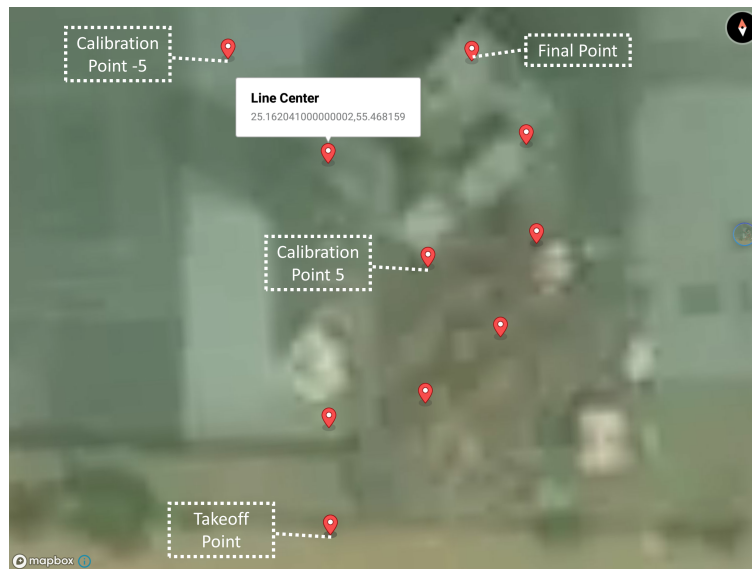

Figure B4. A UI where each waypoint in the mission, calibration points used, and calibration line centre can be reviewed on satellite map.